Stability and chaos around multipolar deformed bodies: A general relativistic approach

Eduardo Guéron* and Patricio S. Letelier†

Departamento de Matemática Aplicada, Instituto de Matemática, Estatística e Computação Científica, Universidade Estadual de Campinas, 13083-970, Campinas, SP, Brazil

The exact solution to the Einstein equations that represents a static axially symmetric source deformed by an internal quadrupole is considered. By using the Poincaré section method we numerically study the geodesic motion of test particles. For the prolate quadrupolar deformations we found chaotic motions contrary to the oblate case where only regular motion is found. We also study the metric that represents a rotating black hole deformed by a quadrupolar term. This metric is obtained as a two soliton solution in the context of Belinsky–Zakharov inverse scattering method. The stability of geodesics depends strongly on the relative direction of the spin of the center of attraction and the test particle angular momentum. The rotation does not alter the regularity of geodesic motions in the oblate case, i.e., the orbits in this case remain regular. We also employ the method of Lyapounov characteristic numbers to examine the stability of orbits evolving around deformed nonrotating centers of attraction. The typical time to observe instability of orbits is analyzed.

I. INTRODUCTION

After the visionary work of Poincaré [1] and the KAM (Kolmogorov, Arnol'd, and Moser [2]) theory it became well established that non-integrability and hence chaos is a general rather than exceptional manifestation in the context of dynamical systems, see for instance [3]. Given this ubiquitous fact, an important issue in astronomical modeling is the study in which extent in phase space chaoticity rises in models that are relevant to describe real systems and what are its consequences.

The adequate description of the gravitation field of an astrophysical object has been an important subject in both relativistic and Newtonian gravity since their origin. The particular case of the gravity associated to an axially symmetric body has played a central role in this discussion. Recently, Merrit [4] found, from detailed modeling of triaxial galaxies, that most of the galaxies must be nearly axisymmetric, either prolate or oblate. In Newtonian theory the gravitational potential of an axially symmetric body can be always represented by its usual expansion in terms of Legendre polynomials (zonal harmonics). The underlying theory in this case is the usual Newtonian Gravitation that for large masses and velocities is known to be less appropriate than Einsteinian General Relativity. In the late case the Newtonian potential is replaced by the spacetime metric and Newton motion equations by geodesics. In General Relativity we have that the solution of the vacuum Einstein equations associated to a static axially symmetric body has a simple form with only two metric functions [5] and one of them admits an expansion in zonal harmonics. For rotating axially symmetric bodies we have a metric with three functions and two of them obey a sigma-model type of partial differential equations for which there are known methods of solution [6].

The change of the particle motion equation and gravitational theory can produce dramatic effects, for instance, test particles moving in the presence of systems of masses that are integrable in Newtonian theory are chaotic in General Relativity, examples are: the fixed two body problem [7,8], and particles moving in a monopolar center of attraction surrounded by a dipolar halo [9]. Also gravitational waves, a non existing phenomenon in the Newtonian realm, can produce irregular motion of test particles orbiting around a static black hole [10,11]. Another distinctive feature of general relativity is the dragging of inertial frames due to mass rotation. This fact is observed, for instance, in the impressive differences of the geodesic motion in Schwarzschild and Kerr geometries [12].

Along this article we shall study the geodesic equations for particles evolving in the space time associated to a center of attraction with a quadrupolar deformation. The solution of the Einstein equations representing this center of attraction – in the static case – can be found in [13] wherein the rather misleading terminology "distorted black hole" was used to refer to such an object. Examples of static centers of attractions with multipolar deformations are: a) A true static black hole (or a dense object) surrounded by a distribution of matter like a ring or a small disk formed by counter-rotating matter, i.e., built by approximately the same number of particles moving clockwise as

*e-mail: gueron@ime.unicamp.br
†e-mail: letelier@ime.unicamp.br

counterclockwise. Even though, this interpretation can be seen as a device to have a static stable configuration there is observational evidence of disks made of streams of rotating and counter-rotating matter [14]. b) An axially symmetric static dense object with either polar deformations or polar jets. In the case a) we have oblate deformations. Also the polar deformations of the Sun and the inner planets in the solar system are oblate. We have prolate deformations in stars with jets and in some galaxy clusters [15]. In the precedent cases, by adding rotation to the central black hole and removing the counter-rotating hypothesis we can have stationary centers of attraction with multipolar deformations.

Geodesic motions for axially symmetric spacetimes representing core-halos system were studied in [16] for bounded motion and in [17] for unbounded motions. The case of a slowly rotating center of attraction with a dipolar halo was considered in [18] . The geodesic chaos for a disk with a central center of attraction was considered in [19]. A core-halo system with NUT (Newman-Unti-Tamburino) charge was also considered [20]. Newtonian [21] and pseudo-Newtonian [22] counter parts of some of this systems has been also studied. In a recent paper – within the Newtonian realm – we studied chaotic motions of test-particles orbiting around a deformed body modeled by a monopolar and an internal quadrupolar term [23].

In this article we dwell in study of geodesic chaos, but now related to internal quadrupole deformations of the attraction center. Note that halos are external multipolar contributions, their strength increases with the distance contrary to the internal ones that decreases with the distance. The quadrupolar contribution usually represents the major deviation to the spherical symmetry. Thus, as a good first approximation, it can model most of the deformed sources.

We shall analyze only bounded motions for specific choices of energy and angular momentum and certain values of quadrupolar strength that we believe will cover all the different typical situations. Due to the symmetry of the problem, one can reduce the geodesic motion to a dynamical system with two degrees of freedom. For such cases, the Poincaré section method is the most appropriated tool to study the geodesics general behavior.

The paper consists of two main parts. In the first one, Sec. II, the exact solution to the Einstein equations that represents a static axially symmetric source deformed by an internal quadrupole is considered. By using the Poincaré section method we numerically study the geodesic motion of test particles. For the prolate quadrupolar case we found chaotic motions contrary to the oblate case where only regular motion was found.

In the second part, Sec. III, the rotation of the attraction center is considered. We first study the metric that represents a rotating black hole deformed by a quadrupolar term. This metric is obtained as a two soliton solution in the context of Belinsky–Zakharov inverse scattering method [24] that generates new solutions from a known one (seed solution). As in the precedent section, geodesics were numerically studied using surfaces of section. The consideration of different cases leads us to conclude that the black hole rotation considerably alters the stability of the system. We obtain that the stability depends strongly on the relative direction of the spin of the center of attraction and the test particle angular momentum. We also found that the rotation does not alter the regularity of geodesic motions in the oblate case, i.e., the orbits in this case remain regular. We conclude, in Sec. IV, with further considerations on the stability of orbits. But, now we employ the method of Lyapunov characteristic numbers following Benettin et al. [25]. We also discuss the typical time to observe instability of orbits and make some final remarks.

II. SCHWARZSCHILD SOLUTION WITH QUADRUPOLE DEFORMATIONS

The metric of the spacetime related to the gravitational field of a static axially symmetric source is the one associated with the Weyl line element,

$$ds^2 = e^{2\psi}dt^2 - e^{2(\gamma-\psi)}(dz^2 + dr^2) - r^2e^{-2\psi}d\varphi^2, \tag{1}$$

where ϕ and γ are functions of r and z only. The range of the coordinates r, z, φ are the usual ones for cylindrical coordinates. It is more convenient to use prolate spheroidal coordinates, u and v, that are related to Weyl coordinates by

$$\begin{aligned} r^2 &= m^2(u^2-1)(1-v^2), \\ z &= muv, \end{aligned} \tag{2}$$

where m is a constant, that will be associated with the mass of the center of attraction. The coordinate v takes values in the interval $[-1, 1]$ (it is essentially a cosine) and u runs from 1 to infinity (it is essentially a radial coordinate). We shall use units such that $c = G = 1$. With no lose of generality we shall also choose $m = 1$. In this new system of coordinates, the metric (1) takes the form ,

$$ds^2 = e^{2\psi(u,v)}dt^2 - e^{-2\psi(u,v)}(u^2-1)(1-v^2)d\phi^2$$
$$-e^{2(\gamma(u,v)-\psi(u,v))}(u^2-v^2)\left(\frac{du^2}{u^2-1}+\frac{dv^2}{1-v^2}\right). \tag{3}$$

For this line element the vacuum Einstein equations reduce to,

$$[(u^2-1)\psi_{,u}]_{,u} - [(1-v^2)\psi_{,v}]_{,u} = 0, \tag{4}$$

$$\gamma_{,u} = \frac{(u\psi_{,u} - 2v\psi_{,v})(u^2-1)(1-v^2)\psi_{,u} - u(1-v^2)^2{\psi_{,v}}^2}{(u^2-v^2)},$$
$$\gamma_{,v} = \frac{(2u\psi_{,u} - v\psi_{,v})(u^2-1)(1-v^2)\psi_{,v} + v(u^2-1)^2{\psi_{,u}}^2}{(u^2-v^2)}. \tag{5}$$

Equation (4) is the usual Laplace equation in prolate coordinates for the metric potential ψ and Eqs. (5) yield the function γ as a quadrature. The ingrability of γ $(\gamma_{,uv} = \gamma_{,vu})$ is guaranteed by Eq. (4). The potential ψ for the Schwarzschild solution in prolate coordinates is [5] ,

$$\psi_S = \frac{1}{2}\log\frac{1-u}{1+u}. \tag{6}$$

In this article we shall consider the solution,

$$\psi = \frac{1}{2}\log\frac{1-u}{1+u} + k_2 P_2(v)Q_2(u), \tag{7}$$

where P_2 and Q_2 are the second Legendre polynomial and function,

$$P_2(x) = (3x^2-1)/2, \;\; Q_2(x) = [P_2(x)\log\frac{x+1}{x-1} - 3x]/2, \tag{8}$$

and k_2 is a constant that is positive (negative) for oblate (prolate) deformations. Note that the Newtonian limit of the potential (7) is [26], $\phi = -m/R + (2m^3k_2/15)P_2(\cos\vartheta)R^{-3}$.

From (5) we find the other metric function,

$$\begin{aligned}\gamma = \{&4[2((7k_2^2 - 20k_2 + 4)\log(u-1) + (k_2+2)^2\log(u+1) - 4\log(u^2-v^2)(k_2-1)^2) - 3((27u^2v^2 - 30u^2 - 21v^2 + \\ &26)k_2 - 8)\log((u+1)/(u-1))k_2uv^2 + 3((27u^2v^4 - 30u^2v^2 + 3u^2 - 12v^4 + 16v^2)k_2 - 16v^2)k_2] - \\ &3[4((3u^2 - 3u - 2)k_2 + 8) - 3(9u^2v^2 - u^2 - v^2 + 1)(u-1)(v^2-1) \\ &\log((u+1)/(u-1))k_2](u+1)\log((u+1)/(u-1))k_2\}/64.\end{aligned} \tag{9}$$

The exact solution to Einstein equations given by (7)-(9) was first study by Erez and Rosen [27], we will comeback to this point latter. The general case (Schwarzschild with the whole series of multipoles) was considered by Quevedo [28] and a simple interpretation in terms of bars was presented by Letelier [29]. This solution has been interpreted as a "distorted" black hole in [13]. The study of the associated Newtonian multipoles as well as the relativistic multipoles for this solution and other multipolar expansion can be found in [30]. The geodesic equations for the metric (3) take the form,

$$\frac{d^2u}{d\tau^2} = \frac{u^2-1}{2e^{2(\gamma-\psi)}(u^2-v^2)}\left(\partial_u e^{2\psi} + \partial_u[(u^2-1)(1-v^2)e^{-2\psi}]\right) - \dot{u}^2\left([\partial_u(\gamma-\psi)] + \frac{(v^2-1)u}{(u^2-v^2)(u^2-1)}\right)$$
$$-2\dot{u}\dot{v}\left([\partial_v(\gamma-\psi)] - \frac{v}{(u^2-v^2)}\right) - \dot{v}^2\left(\frac{(u^2-1)[\partial_u(\gamma-\psi)]}{(v^2-1)} + \frac{(u^2-1)u}{(u^2-v^2)(v^2-1)}\right), \tag{10}$$
$$\frac{d^2v}{d\tau^2} = \frac{1-v^2}{2e^{2(\gamma-\psi)}(u^2-v^2)}\left(\partial_v e^{2\psi} + \partial_v[(u^2-1)(1-v^2)e^{-2\psi}]\right) - \dot{v}^2\left([\partial_v(\gamma-\psi)] - \frac{(u^2-1)v}{(u^2-v^2)(v^2-1)}\right)$$
$$-2\dot{u}\dot{v}\left([\partial_u(\gamma-\psi)] + \frac{u}{(u^2-v^2)}\right) - \dot{u}^2\left(\frac{(v^2-1)[\partial_v(\gamma-\psi)]}{(u^2-1)} - \frac{(v^2-1)v}{(u^2-v^2)(u^2-1)}\right), \tag{11}$$
$$E = e^{2\psi(u,v)}\dot{t}, \;\; L = e^{-2\psi(u,v))}(u^2-1)(1-v^2)\dot{\varphi}, \tag{12}$$

where $\tau = s/c = s$ and the overdots indicate derivative with respect τ. E and L are constants of integrations related to the test particle energy and the angular momentum, respectively. The metric (3) gives a third constant of motion,

$$1 = e^{2\psi(u,v)}\dot{t}^2 - e^{-2\psi(u,v)}(u^2-1)(1-v^2)\dot{\varphi}^2 - e^{2(\gamma(u,v)-\psi(u,v))}(u^2-v^2)\left(\frac{\dot{u}^2}{u^2-1}+\frac{\dot{v}^2}{1-v^2}\right). \tag{13}$$

The motion of the test particle is completely determined by the solution of the two second order differential equations (10) and (11). They define a four dimensional phase space, but the motion constants (13) and (12) tell us that the motion is effectively realized in a three dimensional surface. Moreover, these constants allow us to define an effective potential like function,

$$\Phi(u,v) = \frac{e^{2(\psi(u,v)-v(u,v))}}{(u^2-v^2)}\left(e^{-2\psi(u,v)}E^2 - \frac{e^{2(\psi(u,v)-v(u,v))}}{(u^2-1)(1-v^2)}L^2 - 1\right). \tag{14}$$

Thus the motion must be restricted to the region defined by the inequality $\Phi(u,v) \leq 0$.

Since the geodesic motion of the test particles is performed in a three dimensional effective phase space an adequate tool to study this motion is the Poincaré section method. As we mentioned before the sign of the quadrupole parameter k_2 specifies if the source is deformed in a prolate or in an oblate shape. First we shall study the prolate case, $k_2 < 0$.

From relation (14) we can find the appropriated constants to have a confined motion. We find that only three combinations of the constants: E (energy), L (angular momentum) and k_2 (quadrupole strength), characterize all the possibilities of confinement. In Fig.1 we present the curve $\Phi(u,v) = 0$ for $L = 3.32$, $E = 0.937$ and $k_2 = -5.02$. We have two bounded regions and two unbounded ones. With the same values to L and E and a small change in the quadrupolar constant, $k_2 = -5.0$, we obtain the curve plotted in Fig.2. The two bounded regions merge in a single one. The two escape zones remain unbounded. Finally, in figure 3, we present the curve $\Phi(u,v) = 0$ for $L = 3.8$, $E = 0.9731$ and $k_2 = -1$. Now the two zones of unbounded motion merge in a single one and the region of bounded motions increases.

We construct Poincaré surface sections for the the three sets of constants indicated above. In Fig.4 we present a Poincaré section for the two bounded regions of Fig. 1. In the middle bounded region we have a typical picture of chaotic motion. However the orbits confined in the right hand side bounded region present regular motion. In Fig.5 we show the Poincaré section obtained for orbits restricted to the closed surface presented in Fig.2. It is interesting to observe that we have a region of irregular motion in the left hand side of the graphic very similar to the one showed in the previous figure and in the right hand side a region of regular motion surrounded by a chaotic one.

In Fig. 6 we show that the motion in the bounded region of Fig. 3 is regular as in the case of a pure Schwarzschild black hole [16]. These results can be understood by studying the effective potential critical points. We recall that a pure black hole ($k_2 = 0$) with adequate values of the constants E and L has an effective potential with a single saddle point. When we add the prolate quadrupolar field $k_2 < 0$ we have a second saddle point for the value of the constants of Figs. 1 and 2. In the third case (Fig. 3) the second saddle point disappears and we end up with the same dynamical behavior of the test particles as in the pure Schwarzschild black hole case.

For the case of oblate quadrupole deformation, i.e., $k_2 > 0$, we found regions of bounded motion very similar to the one presented in Fig. 3. But, we did not find a second as in Figs. 1 and 2. This indicates the absence of a second saddle point. We studied surface sections for many different values for E, L and $k_2 > 0$. We always found regular motion.

III. KERR SOLUTION WITH QUADRUPOLE DEFORMATIONS

Since the Kerr solution represents a rotating black hole, the addition of an internal multipole term can be used to model a rotating star or the core of a galaxy. The black hole rotation produces the pure relativistic effect of dragging of inertial frames. Then our main goal, in this section, is to study the influence of the black hole rotation on the stability of geodesic motions. Letelier and Vieira [18] studied the motion of test particles moving around a slowly rotating black hole with a dipolar halo. Now we shall study the case of a central body with arbitrary rotation deformed by an internal quadrupole term.

The metric for a stationary axially symmetric spacetime has the general form,

$$ds^2 = g_{tt}dt^2 + 2g_{t\phi}dtd\phi + g_{\phi\phi}d\phi^2 - e^{\Gamma}(u^2-v^2)\left[\frac{du^2}{u^2-1}+\frac{dv^2}{1-v^2}\right], \tag{15}$$

where g_{tt}, $g_{t\phi}$, $g_{\phi\phi}$ and Γ are function of the coordinates u, v.

Belinsky and Zakharov presented a solution generating algorithm for metrics with two independent Killing vectors [24]. They obtained the Kerr solution by applying the method to the Minkowski spacetime (seed solution). The application of this solution generating method to more general seeds was studied in [31]. Using the techniques presented in this last article we can easily obtain the metric functions $g_{tt}(u,v)$, $g_{t\phi}(u,v)$, $g_{\phi\phi}(u,v)$ and $f(u,v)$ that represent a Kerr black hole deformed by multipolar terms. We choose as the seed a metric representing a pure quadrupole. Then the the two-soliton solutions give us the nonlinear superposition of a Kerr solution with a quadrupolar field. We find,

$$\begin{aligned} g_{tt} = &(e^H(e^{2H}((2e^{2F_1+2F_2}(u^2-v^2)-e^{2H}(v^2-1))(p+1)^2-e^{4F_1}(u+1)(u-1)q^2)q^2\\ &-e^{4F_2}(e^{2H}(p+1)^2(u+1)(u-1)+e^{4F_1}(v^2-1)q^2)(p+1)^2))/\\ &(e^{2H}((2e^{2F_1+2F_2}(u+v)(u-v)-e^{2H}(v-1)^2)(p+1)^2e^{4F_1}(u-1)^2q^2)q^2-e^{4F_2}\\ &(e^{2H}(p+1)^2(u+1)^2+e^{4F_1}(v+1)^2q^2)(p+1)^2), \end{aligned} \tag{16}$$

$$\begin{aligned} g_{t\phi} = &(-2e^H(e^{2H}((2e^{2F_1+2F_2}(u^2-v^2)\\ &-e^{2H}(v^2-1))(p+1)^2-e^{4F_1}(u+1)(u-1)q^2)q^2-\\ &e^{4F_2}(e^{2H}(p+1)^2(u+1)(u-1)+e^{4F_1}(v^2-1)q^2)(p+1)^2+\\ &(e^{2F_1}(e^{4F_2}(p+1)^2(u+1)(v+1)+e^{2H}(u-1)(v-1)q^2)(u-v)-\\ &e^{2F_2}(e^{2H}(p+1)^2(u+1)(v-1)+e^{4F_1}(u-1)(v+1)q^2)(u+v))(p+1)p)q)/\\ &(e^{2H}((2e^{2F_1+2F_2}(u^2-v^2)-e^{2H}(v-1)^2)(p+1)^2-e^{4F_1}(u-1)^2q^2)q^2-\\ &e^{4F_2}(e^{2H}(p+1)^2(u+1)^2+e^{4F_1}(v+1)^2q^2)(p+1)^2), \end{aligned} \tag{17}$$

$$g_{\phi\phi} = \frac{g_{t\phi}^2 - p^2(1-v^2)(u^2-1)}{g_{tt},} \tag{18}$$

$$\begin{aligned} e^{\Gamma} = &-(\exp[((((4(2\log(u+1)+81u^2v^4-90u^2v^2+9u^2-36v^4+48v^2-8\log(u+v)+\\ &14\log(u-1)-8\log(u-v))+9(9u^2v^2-u^2-v^2+1)(u^2-1)(v^2-1)\log((u+1)/(u-1))^2\\ &-12(27u^3v^4-30u^3v^2+3u^3-2-(21v^2-5)(v^2-1)u)\log((u+1)/(u-1)))k_2-\\ &16((3u^2-1)\log((u+1)/(u-1))-6u)(3v^2-1))k_2)/128)](e^{2H}((2e^{2F_1+2F_2}(u^2-v^2)-\\ &e^{2H}(v-1)^2)(p+1)+e^{4F_1}(p-1)(u-1)^2)(p-1)+e^{4F_2}(e^{2H}(p+1)(u+1)^2-e^{4F_1}\\ &(p-1)(v+1)^2)(p+1)))/(4e^{2F_1+2F_2+2H}(u^2-v^2)p^2), \end{aligned} \tag{19}$$

where

$$\begin{aligned} F_1 = &(-(2(2(\log(u+1)-3v^2-3\log(u-1)+2\log(u-v))+3(3v-1)(v+1)u)\\ &+3((v+3+2(v+1)u)(v-1)-(3v-1)(v+1)u^2)\log((u+1)/(u-1)))k_2)/16, \end{aligned} \tag{20}$$

$$\begin{aligned} F_2 = &(-(2(3((3v-1)(v+1)u+2v^2)-4\log(u+v)+4\log(u-1))-\\ &3((3v-1)u-(v+1))(u+1)(v+1)\log((u+1)/(u-1)))k_2)/16 \end{aligned} \tag{21}$$

$$H = (((3u^2-1)\log((u+1)/(u-1))-6u)(3v^2-1)k_2)/8k_2)/8. \tag{22}$$

The quadrupole strength is k_2, q is the source angular momentum per the square of the mass and p is defined by the relation $p^2+q^2=1$. The metric presented above is a particular case of the general solution that represent a Kerr metric embedded in a field of multipoles, see for instance [32] and [29], we will back to this point latter.

When one performs the limit $k_2 \to 0$ in the solution presented above one obtains the Kerr metric in Boyer Lindquist coordinates, r and ϑ that are related to the prolate spheroidal coordinates, u and v by $u=(r-m)/\sigma$ and $v=\cos\theta$. The constant p and q are related to the Boyer Lindquist constants by $p=\sigma/m, \quad q=a/m$, and $m^2=\sigma^2+a^2$. m is the monopole mass, σ is only an auxiliary constant and a is interpreted as the black hole angular momentum per unit of mass measured by a very distant observer.

As in the precedent case, the geodesic equations have two constants of motion, L and E, that obey the relation.

$$g_{tt}\dot{t}+g_{t\phi}\dot{\phi}=E, \quad g_{\phi\phi}\dot{\phi}+g_{t\phi}\dot{t}=L. \tag{23}$$

The evolution equations for u and v are

$$\frac{d^2u}{d\tau^2} = \frac{u^2-1}{2\Gamma(u^2-v^2)}\left[\partial_u g_{tt}\dot{t}^2 + 2\partial_u g_{t\phi}\dot{t}\dot{\phi} + \partial_u g_{\phi\phi}\dot{\phi}^2\right] - \dot{u}^2\left[\frac{\partial_u\Gamma}{2\Gamma} + \frac{(v^2-1)u}{(u^2-v^2)(u^2-1)}\right]$$
$$-2\dot{u}\dot{v}\left[\frac{\partial_v\Gamma}{2\Gamma} - \frac{v}{(u^2-v^2)}\right] - \dot{v}^2\left[\frac{\partial_u\Gamma(u^2-1)}{2\Gamma(v^2-1)} + \frac{(u^2-1)u}{(u^2-v^2)(v^2-1)}\right], \tag{24}$$

$$\frac{d^2v}{d\tau^2} = \frac{1-v^2}{2\Gamma(u^2-v^2)}\left[\partial_v g_{tt}\dot{t}^2 + 2\partial_v g_{t\phi}\dot{t}\dot{\phi} + \partial_v g_{\phi\phi}\dot{\phi}^2\right] - \dot{v}^2\left[\frac{\partial_v\Gamma}{2\Gamma} - \frac{(u^2-1)v}{(u^2-v^2)(v^2-1)}\right]$$
$$-2\dot{u}\dot{v}\left[\frac{\partial_u\Gamma}{2\Gamma} + \frac{u}{(u^2-v^2)}\right] - \dot{u}^2\left[\frac{\partial_v\Gamma(v^2-1)}{2\Gamma(u^2-1)} - \frac{(v^2-1)v}{(u^2-v^2)(u^2-1)}\right]. \tag{25}$$

As in the precedent case we have two second order evolution equations (24) and (25) for the variables u and v, the metric and the constants (23) give a new constant relating these two variables,

$$1 = g^{tt}E^2 + 2g^{t\phi}EL + g^{\phi\phi}E^2 - e^{\Gamma}\left(u^2-v^2\right)\left[\frac{\dot{u}^2}{u^2-1} + \frac{\dot{v}^2}{1-v^2}\right]. \tag{26}$$

In other words, despite algebraic complications, we have exactly the same dynamical situation as before. The particles move in an effective three dimensional space. Thus we shall analyze the motion of test particles moving in the gravitational field of a rotating prolate deformed body using Poincaré sections as in the non-rotating case.

Since the main new ingredient in the new system is the rotation of the source we shall keep the angular momentum L, the energy E and the quadrupole strength k_2 fixed and we shall consider test particles moving with angular momentum parallel to the spin source (co-rotation) and with angular momentum anti-parallel to the spin source (counter-rotation).

In Fig.7 we present the region of bounded motions for counter-rotating orbits, $qL < 0$. We take $E = 0.93715$, $|L| = 3.322$, and $k_2 = -5.08$, and for the rotation parameter, $q = 0.002$. We notice a situation similar to the one presented in Fig.2. The bounded regions for the co-rotation case, $qL > 0$ is shown in Fig.8. We see two relatively small and distant closed surfaces. The Poincaré section for the counter-rotating case is presented in Fig.9. Chaotic motion can be perceived in the left hand side of the graphic and in the external part of the right hand side as in Fig.5. In Fig.10 we present the surface section for the same parameters as above, but $qL > 0$ (co-rotation). We do not find chaotic motion in this case.

We were not able to obtain bounded motion for both large quadrupole strength and large rotation parameter. We studied bounded systems with large rotation speed (of the order of 0.1) but with quadrupole strength always less than unit. In these cases the study of Poincaré sections leads to regular geodesic motion for co-rotation, as well as, counter-rotation. We also found that the confinement region may suffer an appreciable change in size and shape.

IV. DISCUSSION

As we said before, the exact solution to Einstein equations presented in the two precedent sections are not new and different versions of them have already appear in the literature. We have presented them in this work for two reasons: a) For easy reference, and b) Mainly, because for numerical analysis we need a faultless solution. The one presented here were derived using algebraic computation and checked using the full vacuum Einstein equations in each case.

Besides the Poincaré section, we have another technique to quantify geodesic instability: the Lyapunov characteristic number, $\mathcal{N}$, defined as,

$$\mathcal{N} = \lim_{\substack{\delta_0 \to 0 \\ \tau \to \infty}} \left[\frac{\log(\delta/\delta_0)}{\tau}\right], \tag{27}$$

where δ_0 and δ are the deviation of two nearby orbits at times 0 and t respectively. Using the technique suggested by Benettin et al. [25] – who studied numerical problems in the computation of Lyapunov exponents and Kolmogorov entropy – one can get the largest $\mathcal{N}$.

Using the constants that define the bound region presented in Fig. 1 we obtain $\mathcal{N} = (9.0 \pm 1.0) \times 10^{-17}$, where the maximum $\mathcal{N}$ was obtained for $u = 2.6$, $v = 0$ and $p_v = 0$. In the right region plotted in Fig. 4 we get always $\mathcal{N} < 5 \times 10^{-18}$. This shows, as expected, that the Lyapunov coefficient in the regions with chaotic motion does not vanish while in the region with irregular motion it could vanish. Nevertheless, the value of the coefficient for chaotic motions is very small, it means that the dispersion of the orbits is slow if compared with local fluctuations in the mean potential.

We found chaotic geodesic motions for the system black hole plus internal quadrupole for a very small range of parameters, specifically when there is a second bounded region. When one considers a rotating source one just re-obtained the same behavior studied in [18] for rotating centers of attraction with halos. The orbits of counter-rotating particles are more unstable that the orbits for corotating particles. In reference [18] the case of slow rotation was considered.

We also studied some bounded chaotic motion for large rotation speed ($q > 0.1$) in a Kerr halo system from an exact solution that represents an external dipole plus a Kerr black hole. Using the techniques presented in this paper we conclude that the irregularity introduced by external multipole terms are much larger than the ones introduced by internal multipole terms. We found also that chaotic motions for large rotation speed are more frequently, i.e., we have irregular motion for a larger range of the constants E and L.

It is not easy to predict the role that chaos could have in measurable characteristics of galaxies. Let us choose a parameter $\mathcal{T}$ as the time to characterize the dynamics of the system e.g., to draw the sections of an invariant torus in a regular motion or a chaotic region in the Poincaré section for irregular motion. We shall consider that this is the minimum time to have observable effects.

Rearranging the units to observable parameters, we obtain $\mathcal{T}$ in years from the expression

$$\mathcal{T} = N \times M \times 1.6 \times 10^{-13} yr,$$

where N is the number of steps in the simulations and M is the mass of the central black hole (in solar masses). The step N varies for different systems. It is about 10^4 for a black hole plus halo system and about 10^{16} for a black hole plus internal quadrupole system. For a typical galactic bulge we have $M = 10^{12} M_{\odot}$. Then for black hole plus halo system we have $\mathcal{T} = 1000yr$ which is a very small value when compared with galactic ages and for the black hole plus internal quadrupole system, $\mathcal{T} = 10^{15} yr$ which is a very large value compared with the Universe age ($10^{10} yr$). Consequently, chaotic relativistic effect may show up in the formation of structures in a black hole plus external halo system, work along this line will soon be reported. The relativistic effect due to the rotation of the source may be important. The internal deformations do not have a significant contribution in this case. Another possible observational manifestation of chaos was studied in [33]

Acknowledgements. The authors thank FAPESP for financial support. PSL also thanks CNPq.

---

[1] H. Poincaré *Les Méthodes Nouvelles de la Mechanique Celeste,* (Gauthier-Villars, Paris, 1892)

[2] A.N. Kolmogorov, Dokl. Akad. Nauk. SSSR, 98, 527 (1954). V.I. Arnol'd., Russ. Math. Surv. 18, 9 (1963); ibid 18, 85 (1963). J. Moser,Math. Ann., 169, 136 (1967)

[3] M.V. Berry, Am. Inst. Phys. Conf. Proc. 46, 16 (1978)

[4] D. Merrit, Science 271, 337 (1996)

[5] See for instance, H. Robertson and T. Noonan, "Relativity and Cosmology"(Saunders, London 1968) pp 272-278.

[6] See for instance, C.M. Cosgrove, J. Math. Phys. 23, 615 (1982) and references therein.

[7] G. Contopoulos, Proc. R. Soc. Lond. A 431, 183 (1990); A 435, 551 (1991).

[8] Y. Sota, S. Suzuki and K. Maeda, Class. Quantum Grav. 13, 1241 (1996). See also, W.M. Vieira and P.S. Letelier, Class. Quantum Grav. 13, 3115 (1996).

[9] W.M. Vieira and P.S. Letelier, Phys. Lett. A, 288, 22 (1997).

[10] L. Bombelli and E. Calzetta, Class. Quantum Grav. 9, 2573 (1992).

[11] P.S. Letelier and W.M. Vieira, Class. and Quantum Grav., 14, 1249 (1997).

[12] S. Chandrasekhar, "The mathematical theory of black holes", (Clarendon Press, Oxford, 1983).

[13] See for instance, Ya. B. Zeldovich and I.D. Novikov, "Relativistic Astrophysics" (University of Chicago Press, Chicago 1971) pp 130-134; M. Carmeli, "Classical Fields: General Relativity and Gauge Theory" (John Wiley, New York 1982) pp 177-182.

[14] F. Bertola *et al.*, Ap. J. 458, L67 (1996).

[15] A. R. Cooray, Mon Not. R. Astron. Soc. **313**, 783 (2000).

[16] W. M. Vieira and P. S. Letelier, Ap. J 513, 383 (1999); Phys. Rev. Lett. 76, 1409 (1996).

[17] A.P.S. Moura and P.S. Letelier, Phys. Rev. E, 61, 6506 (2000).

[18] P.S. Letelier and W.M. Vieira, Phys. Rev. D 56,8098 (1997).

[19] A. Saa and R. Venegeroles, Phys Lett A 259, 201 (1999); see also, A. Saa, Phys Lett A **269**, 204 (1999).

[20] P.S. Letelier and W.M. Vieira, Phys. Lett. A, 244, 324 (1998).
[21] A.P.S. Moura and P.S. Letelier, Physics Letters A, 266, 309 (2000); P.S. Letelier and W.M. Vieira, Phys. Lett. A, 242, 7 (1998). P.S. Letelier and A.E. Motter, Phys. Rev. E 60, 3920 (1999).
[22] E. Gueron and P.S. Letelier Astron. Astrophys. 368, 716 (2001); H. Varvoglis and D. Papadopoulos, Astron. Astrophys. 261, 664 (1992); V. Karas and D. Vokrouhlicky, Gen. Rel. Gravit. 24, 729 (1992).
[23] E. Gueron and P.S. Letelier, Phys. Rev. E 63 , 035201(R) (2001).
[24] V. A. Belinsky and V. Zakharov, Sov Phys. JETP **50**, 1 (1979)
[25] G. Benettin, L. Galgani and JM. Streclyn, Phys. Rev. A **14** 2338 (1976)
[26] J. Ehlers, in "Grundlagenprobleme der Modernen Physik", A. Erdélyi, J.Pfarr, and E.-W. Stachov, Eds. (BI-Verlag, Mannheim, 1981) pp 65-84.
[27] G. Erez and N. Rosen, Bull. Res. Counc. Isr. 8F, 47 (1959).
[28] H. Quevedo, Phys Rev. D **39** 2904 (1989)
[29] P.S. Letelier, Class. Q. Grav., 16, 1207 (1999).
[30] B. Boisseau and P.S. Letelier " Relativistic Multipoles and the Advance of the Perihelia", preprint Université de Tours (2001).
[31] P. S. Letelier, J. Math Phys. 26, 467 (1984)
[32] H. Quevedo and B. Mashhoon, Phys Rev. D 43, 3902 (1991)
[33] J. Levin, Phys. Rev. D **60**, 4015 (1999)

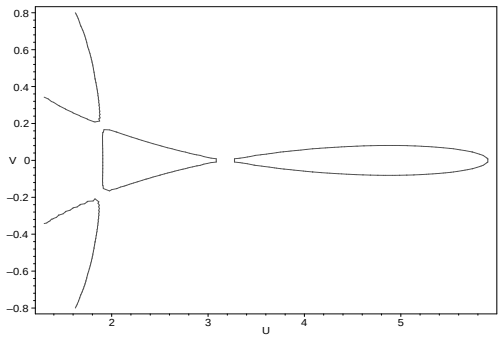

FIG. 1. Boundary contour ($\Phi = 0$) for a static black hole + quadrupole system $L = 3.32$, $E = 0.937$ and $k_2 = -5.02$. There are two escape zones in the left hand side of the picture that corresponds to small values of u and a couple of closed zones of bounded motion.

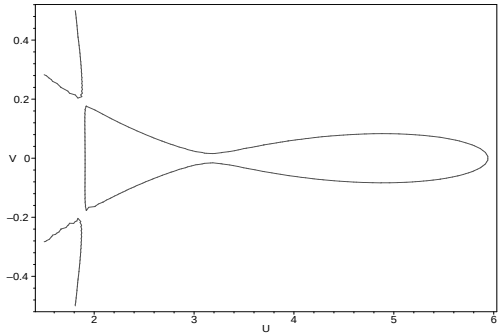

FIG. 2. Boundary of contour for the same values for L and E but $k_2 = -5.0$. The two escape zones remain. However, the two closed zones merge in only one.

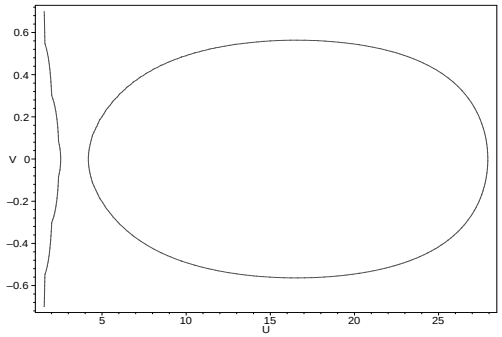

FIG. 3. Boundary contour for $L = 3.8$ and $E = 0.973$ but $k_2 = -1.0$. No vestige of the second bounded region is left.

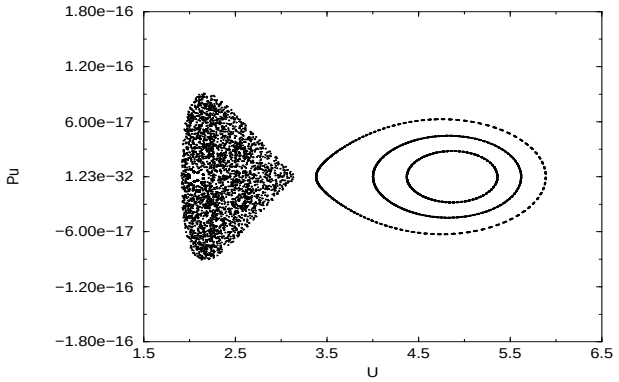

FIG. 4. Poincaré Section for the values defined in Fig.1. We see chaotic behavior in orbits confined in the first zone of bounded motions. But, the motion in the second zone is regular

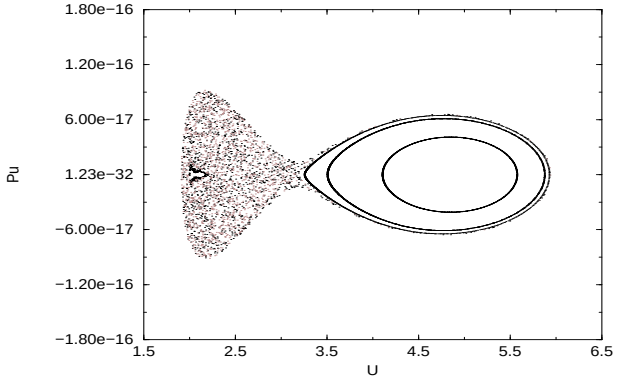

FIG. 5. Poincaré Section for the values defined in Fig.2. We see chaotic motion in the left hand side of the figure and in a small external region of the right hand side.

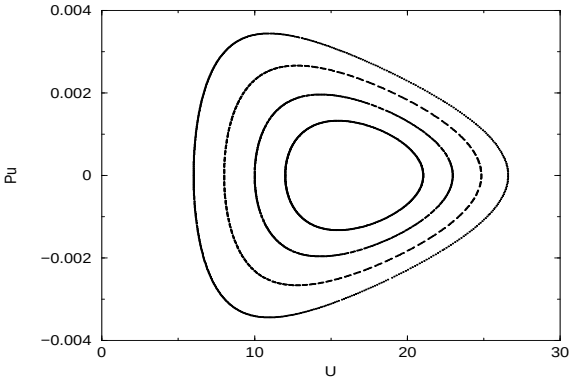

FIG. 6. Poincaré Section for the values defined in Fig.3. We have regular motion.

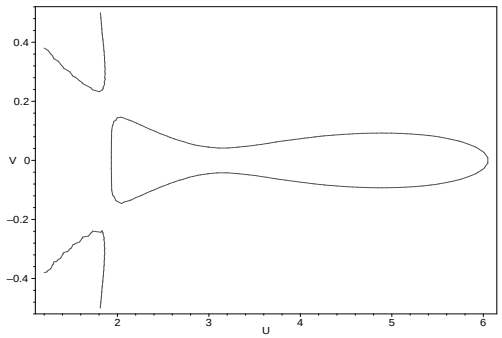

FIG. 7. Boundary contour of the Kerr+Quadrupole system for $L = -3.322$, $E = 0.93715$, $k_2 = -5.08$ and $q = 0.002$.

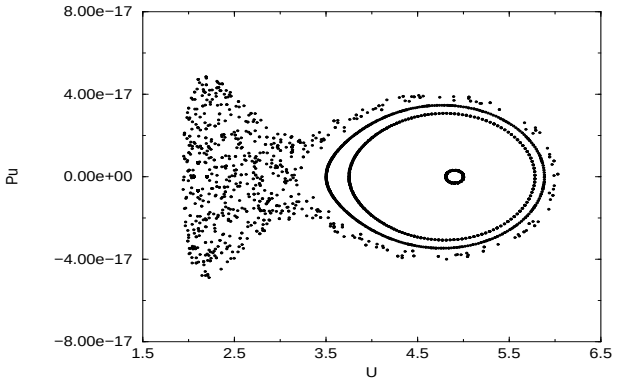

FIG. 9. Poincaré Section for the same value of the parameters of Fig. 7. We have chaotic motion mainly in the left hand side of the picture

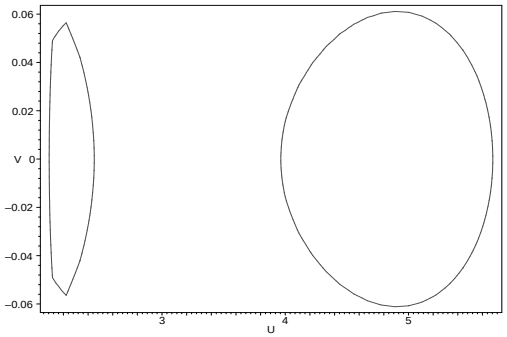

FIG. 8. Boundary contour of the Kerr+Quadrupole system for $L = 3.322$, $E = 0.93715$, $k_2 = -5.08$ and $q = 0.002$. The confinement region is separated in two. They are much smaller than in the precedent figure

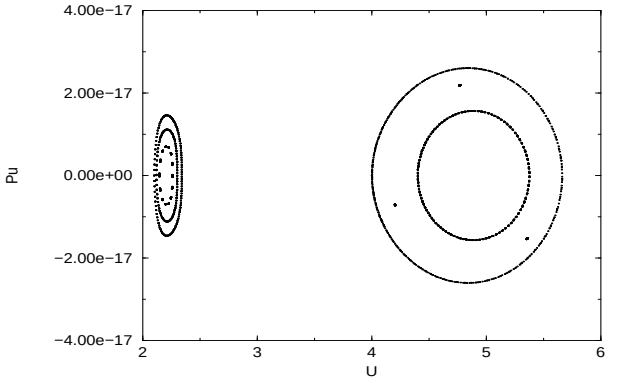

FIG. 10. Poincaré Section for the same value of the parameters of Fig. 8. We do not see irregular motion in both regions